Correlation energy of the uniform electron gas determined by ground-state conditional probability density functional theory

Dennis Perchak [*] and Ryan J. McCarty [†]

Department of Chemistry, University of California, Irvine, California 92697, USA

Kieron Burke [‡]

Department of Chemistry, University of California, Irvine, California 92697, USA
and Department of Physics and Astronomy, University of California, Irvine, California 92697, USA

Conditional-probability density functional theory (CP-DFT) is a formally exact method for finding correlation energies from Kohn-Sham DFT without evaluating an explicit energy functional. We present details on how to generate accurate exchange-correlation energies for the ground-state uniform gas. We also use the exchange hole in a CP antiparallel spin calculation to extract the high-density limit. We give a highly accurate analytic solution to the Thomas-Fermi model for this problem, showing its performance relative to Kohn-Sham and it may be useful at high temperatures. We explore several approximations to the CP potential. Results are compared to accurate parametrizations for both exchange-correlation energies and holes.

I. INTRODUCTION

The uniform electron gas (UEG) plays an iconic role in condensed matter physics [1]. It is the simplest example of an interacting electronic system in the thermodynamic limit. It has also been used as a simple model for metals, especially simple metals like Na and Al [2]. Moreover, its exchange-correlation (XC) energy is a vital input to the local density approximation (LDA) for inhomogeneous systems, an approximation that dominated density functional theory (DFT) calculations for a generation, and remains in wide use today [3]. The ground-state energy was first calculated accurately by Ceperley and Alder [4], and modern parametrizations largely agree at the 1% level [5–7]. On the other hand, the finite temperature case is still actively being calculated today [8–10].

Recently, it was pointed out that, for any electronic system, one could extract the unknown XC energy by a sequence of Kohn-Sham DFT (KS-DFT) calculations (one for each point on a grid in the system) if a well-defined but unknown potential, the conditional probability potential, were known [11]. A simple LDA to this potential yields surprisingly accurate results for systems as disparate as the binding energy curve of H_2 and the uniform gas. This approximation automatically has no self-interaction error for one-electron systems [6], correctly dissociates the H_2 singlet into two separate H atoms [12], and its accuracy does not deteriorate as the temperature is raised in a uniform gas [11]. Conditional-probability (CP)-DFT relies on a typical KS calculation producing an accurate density, but it is well-established that in most cases, such densities are very accurate [11]. Moreover, the XC energy extracted from such CP densities involves a double-integral that hides imperfections.

However, many questions were left unexplored in the original publication. The formal underpinnings, for any quantum system, are presented elsewhere [13]. In the present work, we focus exclusively on the uniform gas at zero temperature. We give details on how CP calculations are performed, which differ substantially from a traditional DFT calculation, both in the nature of the external potential and the boundary conditions. We first perform the crudest possible CP calculation, by adding a simple Coulomb repulsion at the reference point. This is called a blue electron approximation, thinking of the reference electron as distinguishable from all others (painted blue). The CP is approximated as the ground-state density of an $N − 1$-electron system with the blue electron treated as an external potential generating a simple Coulomb repulsion. This scheme works remarkably well for densities with Wigner-Seitz radii, $r_s > 2$, with errors of less than 12% for the XC energy. However, it fails badly at high densities where exchange dominates, and so is poorly modeled by a classical approximation. Essentially, the on-top exchange hole and its environs is about minus half the density for an unpolarized gas, while the blue electron potential digs almost no on-top hole at all.

We next show how this difficulty was overcome in Ref. [11]. First, the pure blue electron approximation was shown to violate the electron-electron cusp condition by a factor of 2. When this is restored, accurate results for highly quantum systems were achieved, but it has little or no impact on the high-density uniform gas. Then, a large repulsive Gaussian was added to the CP potential, with parameters chosen to reproduce the exchange hole, i.e., essentially an accurate CP potential in this limit. A key principle of our

---

[*]dperchak@icloud.com
[†]rmccarty@uci.edu
[‡]kieron@uci.edu

method is to recover accurate XC energies by performing only single-particle KS calculations, albeit at every point in the system. As finding the exchange hole does not require any many-body calculations, this is deemed acceptable. But it was also necessary to smoothly turn this Gaussian off as a function of increasing r_s, a somewhat empirical procedure, but one which yields the high accuracy presented in Ref. [11].

Here, we bypass this messy procedure, but still without using any many-body results for the uniform gas. We present a more sophisticated and satisfactory solution, by performing a CP calculation for antiparallel spin only, fixing the parallel CP density to that of exchange (which has long been known analytically [14]). By construction, this recovers the correct exchange in the high-density limit, and yields reasonable accuracy for all other r_s, but is less accurate in the low density limit. Combining this procedure at high densities with the original calculation at low densities yields an accurate curve for all r_s values.

Lastly, we consider the Thomas-Fermi (TF) solution to the blue electron problem, and evaluate its accuracy relative to a full KS calculation. We solve the TF equation analytically using a high-density approximation, which turns out to be remarkably accurate for all densities. For atoms, inaccurate TF densities are the chief source of error in TF energies. But here we are calculating a simple impurity in an otherwise uniform background, thereby avoiding evanescent regions, etc. Moreover, since the XC energy involves a double spatial integral in general (and a single integral), it may be more forgiving of errors than an explicit density functional might be. We find that TF CP densities yield reasonably accurate XC energies in CP theory, and their accuracy improves with increasing r_s. We expect TF-CP calculations to be particularly useful at temperatures beyond which the KS equations fail to converge, a regime which inspired many of these ideas (see Ref. [15] and subsequent work).

II. THEORY

A. Background

Standard KS-DFT calculations solve the KS equations within some approximation for the XC energy as a functional of the density, $E_{xc}[n]$:

$$\left[-\tfrac{1}{2}\nabla^2 + v_s[n](\mathbf{r})\right]\phi_i(\mathbf{r}) = \varepsilon_i\,\phi_i(\mathbf{r}), \qquad (1)$$

where ϕ_i are the KS orbitals and ε_i the eigenvalues. Hartree atomic units are used throughout. The KS potential is given by

$$v_s[n](\mathbf{r}) = v(\mathbf{r}) + v_{HXC}[n](\mathbf{r}), \qquad (2)$$

where $v(\mathbf{r})$ is the original one-body potential while $v_{HXC}(\mathbf{r})$ includes the Hartree potential and an XC contribution, $v_{xc}(\mathbf{r}) = \delta E_{xc}[n]/\delta n(\mathbf{r})$. In practice, spin-DFT is used. Most calculations of total energies yield densities sufficiently close to the exact density that the error in the total energy is dominated by the error in E_{xc} itself, rather than on its evaluation on the approximate density [16]. While there have been many improvements and refinements in such approximations over the last half century, there are many known systematic limitations of present-day functionals, such as their inability to correctly

dissociate bonds (strong correlation effects) and electron self-interaction errors [17].

Recently, CP-DFT, an alternative approach to electronic structure calculation, was suggested [11]. This takes advantage of the well-known expression for the XC energy in terms of the (coupling-constant averaged) XC hole, which in turn is simply related to the conditional probability density for finding an electron at $\mathbf{r}'$, given an electron at $\mathbf{r}$. Knowledge of this function (or in fact just some particular integrals over it) determines E_{xc} exactly. The aim in CP-DFT is to *calculate* this CP probability density using a standard KS calculation at every point $\mathbf{r}$ in the system. In principle, if it exists, there is a unique correction to the one-body potential such that the ground-state of $N-1$ electrons yields the desired CP density [18]. In practice, we find a simple LDA works very well most of the time, as our results show.

Thus, writing

$$E_{xc} = \frac{1}{2}\int_0^1 d\lambda \int d^3r \int d^3r' \, \frac{n(\mathbf{r})n_{xc}^\lambda(\mathbf{r},\mathbf{r}')}{|\mathbf{r}-\mathbf{r}'|}, \qquad (3)$$

where integrating over λ is the adiabatic connection between the KS system at $\lambda = 0$ and interacting system at $\lambda = 1$ [19]. The XC hole density is determined via

$$n_{xc}^\lambda(\mathbf{r},\mathbf{r}') = \tilde{n}_{\mathbf{r}}^\lambda(\mathbf{r}') - n(\mathbf{r}'), \qquad (4)$$

where $\tilde{n}_{\mathbf{r}}^\lambda(\mathbf{r}')$ is the conditional probability density for finding an electron at $\mathbf{r}'$, given an electron at $\mathbf{r}$, at coupling strength λ. We define the CP potential as the potential that has ground state density $\tilde{n}_{\mathbf{r}}^\lambda(\mathbf{r}')$ for $N-1$ electrons. It can be written as $v[\tilde{n}_{\mathbf{r}}^\lambda](\mathbf{r}')$, where $v[n](\mathbf{r})$ is the functional dependence of the potential on the ground state density, first described by Hohenberg and Kohn [18]. We then define

$$\Delta\tilde{v}_{\mathbf{r}}^\lambda(\mathbf{r}') = v[\tilde{n}_{\mathbf{r}}^\lambda](\mathbf{r}') - v^\lambda(\mathbf{r}') \qquad (5)$$

as the correction to the external potential needed to yield the CP potential. This is a functional of the original (N-electron) gas density $n(\mathbf{r})$, by the Hohenberg-Kohn theorem [18].

This theory is formally exact if the potential exists, but the exact CP potential is not known in general and must be approximated. A simple approximation, $\Delta\tilde{v}_{\mathbf{r}}^\lambda = \lambda/|\mathbf{r}-\mathbf{r}'|$, accounts for the majority of the CP correlation, and becomes exact as the distance between $\mathbf{r}$ and $\mathbf{r}'$ increases. This can be considered the correct potential in the classical limit, in which particles can be distinguished from one another, and where the missing electron provides a simple Coulomb repulsive impurity potential.

But this cannot be exact for quantum systems in general. For example, recovery of the electron-electron cusp conditions at small $|\mathbf{r}-\mathbf{r}'|$ distances requires instead $\lambda/(2|\mathbf{r}-\mathbf{r}'|)$. A simple interpolation between small and large distances, depending locally on the density, yields

$$\Delta\tilde{v}_{\mathbf{r}}^\lambda[n](\mathbf{r}') \approx \frac{\lambda}{2|\mathbf{r}-\mathbf{r}'|}\left(1 + \mathrm{Erf}\left(\frac{|\mathbf{r}-\mathbf{r}'|}{r_s(n(\mathbf{r}))}\right)\right), \qquad (6)$$

where $r_s = (3/(4\pi n))^{1/3}$ is the Wigner-Seitz radius of the gas density at the reference point, and provides a simple approximation that is correct in both limits [11]. While this mirrors the longstanding challenge of approximating E_{xc} with a density functional, DFT methods often produce

highly accurate densities even when their energies are incorrect [16], allowing CP-DFT to produce accurate solutions for several systems that are challenging for standard DFT methods.

For those familiar with classical DFT of distinguishable particles, this procedure is very like the Percus-Yevick closure [20] of the Ornstein-Zernike equation [21]. In the truly classical case, the blue electron approximation would be exact, if the exact inhomogeneous XC functional were used when solving the KS equations for the impurity. In practice, we expect the use of approximate XC in such calculations to produce only very slight errors, much of which will be forgiven by the multiple integrals in Eq. (3). Moreover, we anticipate that errors will reduce as the density becomes lower, the electrons become more spread out, and the behavior is dominated by pure Coulomb repulsion. Likewise, in the high density limit, we expect difficulties, where the entirely nonclassical exchange effect dominates.

This paper reports only results for the uniform gas at zero temperature. It gives the full details of the potentials and computational methods that were used in Ref. [11], plus an extension of the method used there to extract spin-decomposed holes, and better justify the smooth turn-off of the exchange barrier needed to recover the high-density limit. We also discuss the quasianalytic solution of the Thomas-Fermi equation (instead of the KS equations) for this case. This is of interest, as clearly a TF solution is far less computationally expensive than the KS approach. In cases where the additional cost of solving KS equations at every point is prohibitive, use of TF theory may provide a practical alternative, but only if errors are not substantially increased.

III. METHODS

A. CP-DFT

We now consider applying the CP concept to the spin unpolarized uniform electron gas. By symmetry, the CP potential is spherical, and we perform calculations within a finite sphere of radius R. Because the UEG is translationally invariant, we choose $r = 0$ for the reference point. Further, we drop the prime from r', so that r now denotes the distance from the reference point, as is conventional for UEG calculations. In practice, we perform calculations in a finite sphere with a large but finite number of electrons N. The boundary of the sphere produces nonuniformities in the density, which are minimized by a judicious choice of boundary condition, Eq. (A12). Moreover, by calculating our XC hole density, Eq. (A13), by subtracting densities with N and $N-1$ electrons, the effect of nonuniformity near the surface largely cancels. Thus all our calculations are converged with respect to the size of the sphere. The systems have a maximal radial coordinate R, volume of $V = 4\pi R^3/3$, and average electron density of $\bar{n} = N/V$ and $(N-1)/V$. The KS equations are solved in the LDA for both systems. The potential used in the KS equations is

$$v_{\mathrm{S}}[n](\mathbf{r}) = v_{\mathrm{n}}[n_0](\mathbf{r}) + \Delta\tilde{v}[n](\mathbf{r}) + v_{\mathrm{H}}[n](\mathbf{r}) + v_{\mathrm{XC}}[n](\mathbf{r}),$$
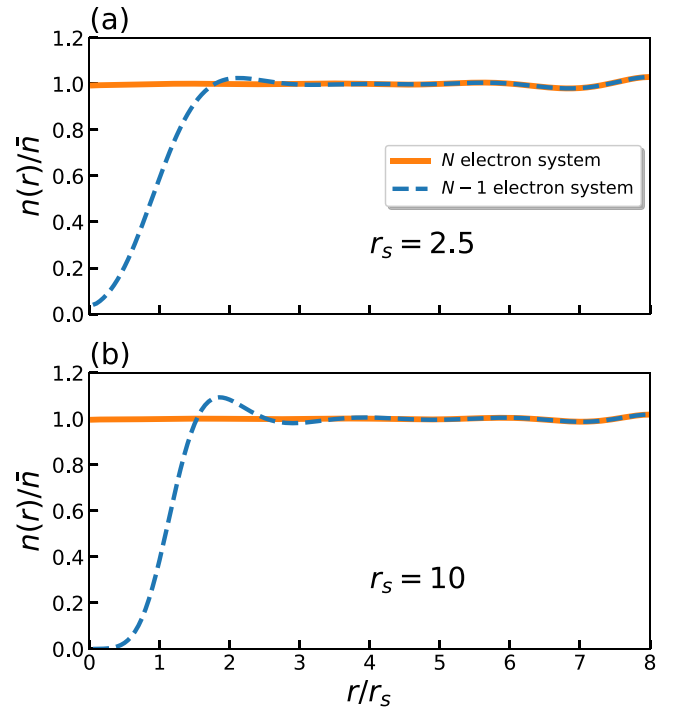
(7)

FIG. 1. Normalized density vs r/r_s for (a) $r_s = 2.5$ and (b) $r_s = 10.0$. Solid line is the N-electron system and the dashed line is the blue electron, $N-1$ system.

where $v_{\mathrm{H}}[n](\mathbf{r})$ is a Hartree repulsion

$$v_H(r) = \int d^3r' \frac{n(\mathbf{r}')}{|\mathbf{r} - \mathbf{r}'|},$$

(8)

and $v_{\mathrm{n}}[n_0](\mathbf{r})$ is a potential derived from a uniform, positive compensating background charge density, $n_0 = N/V$. The exchange-correlation potential, $v_{\mathrm{XC}}[n](\mathbf{r})$ is from LDA using the PW92 parametrization [7]. Lastly, we have the CP or blue potential, which appears only in the $N-1$ electron calculation for which we will consider two forms,

$$\Delta\tilde{v}(r) = \begin{cases} \dfrac{1}{r} & \text{(9a)} \\[2ex] \dfrac{1}{2r}\left(1 + \mathrm{Erf}\left(\dfrac{r}{\bar{r}_s}\right)\right). & \text{(9b)} \end{cases}$$

Here, $\bar{r}_s$ refers to the Wigner-Seitz radius of the system as a whole. As was discussed in the introduction, the simple approximation of $1/r$ for the CP potential is not sufficient for quantum systems. However, it is still instructive to see where it fails. Further details of the CP-DFT and the numerical solution method are contained in Appendix A.

B. CP-DFT results

We first show results for calculations at $r_s = 2.5$ and $r_s = 10.0$ using the simple $1/r$ potential, Eq. (9a), for the blue electron. Figure 1 plots the density of the N electron system and the $N-1$ electron system as a function of the radial coordinate for these two values of r_s. The blue system density in both cases is depressed near $r = 0$ by the repulsion as we would expect. The density difference is the XC hole (at $\lambda = 1$)
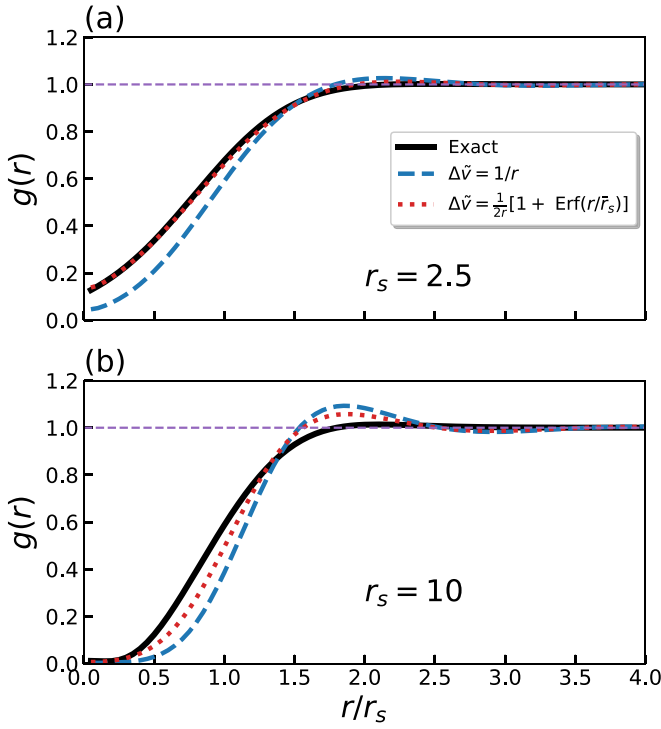
FIG. 2. Pair distribution function, $g(r)$ plotted vs r/r_s for (a) $r_s = 2.5$ and (b) $r_s = 10.0$. The dashed blue line is for the CP potential equal to $1/r$, the dotted red line is for the modified CP Potential and the solid black line is the exact solution.
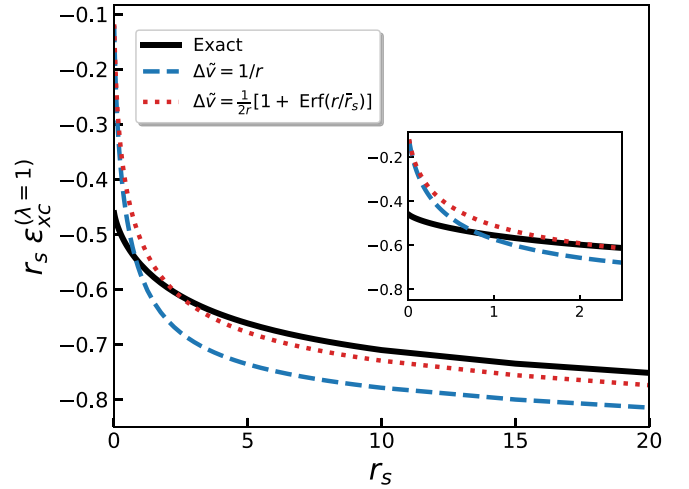

FIG. 3. $r_s \varepsilon_{xc}^{(\lambda=1)}$ vs r_s for the CP potential equal to $1/r$ (dashed blue line), modified CP potential (dotted red line) and the exact solution (solid black line). The inset shows an expanded view of the region for $r_s \gtrsim 2.0$.

C. Spin CP-DFT

In this section, we perform a spin CP-DFT calculation instead of a CP-DFT calculation, showing that the high-density limit can be treated accurately by this method.

The spin conditional probability densities for a system are defined as the probability density for finding an electron at $\mathbf{r}'$, given an electron *of spin* σ at $\mathbf{r}$. Spin conditional probability densities are total densities (not spin densities), but are conditional on an electron having a given spin as well as given position [13]. We can further decompose a spin CP density into a sum of two spin densities. Choosing the blue electron to have spin up (arbitrarily), we write

$$\tilde{n}_{\mathbf{r}\uparrow}(\mathbf{r}') = \tilde{n}_{\mathbf{r}\uparrow}(\mathbf{r}' \uparrow) + \tilde{n}_{\mathbf{r}\uparrow}(\mathbf{r}' \downarrow). \qquad (10)$$

The first is the parallel spin CP spin density, the latter being the antiparallel. We perform a spin KS-DFT calculation in which the former is fixed at its exchange form, which is
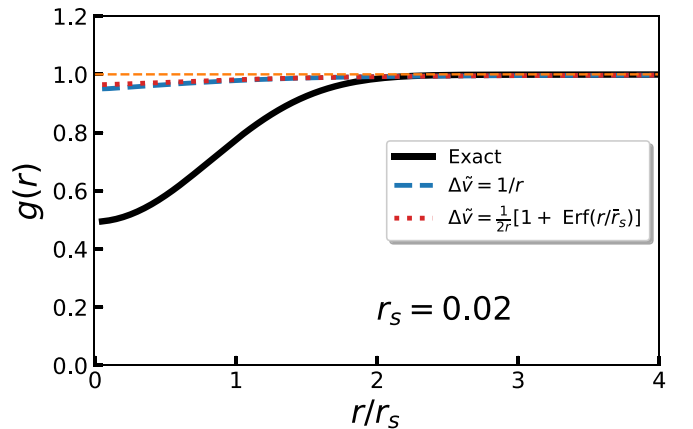
from which one deduces the pair distribution function (PDF), with Eqs. (A13) and (A14). This is shown in Fig. 2 where we have also included calculations for the modified CP potential Eq. (9b). The advantage of calculating both the N and $N-1$ electron systems is apparent in the cancellation of boundary effects. The modified CP potential is significantly better than the simple $1/r$ potential. We can use Eq. (A15) to evaluate the XC energy. This energy is *not* averaged over the coupling constant, i.e., it is the potential contribution only. This is well-known to yield only that part of the XC energy due to electron-electron repulsion, called the potential contribution, while the kinetic contribution is folded in via the coupling-constant integration [22]. Figure 3 shows r_s times the potential XC energy $\varepsilon_{xc}^{(\lambda=1)}$ plotted vs r_s for the same blue potentials as before, along with the exact values. The latter is calculated using the PW92 expressions for $g(r)$ along with Eq. (A14) and Eq. (A15). For values of $r_s \gtrsim 2.5$, the modified blue potential does much better than the simple Coulomb potential, with relative errors less than 3% and 11%, respectively. However, both do badly as the system density increases ($r_s \to 0$), as shown for $r_s = 0.02$ in Fig. 4. The model fails to adequately depress the density near $r = 0$. This is due to the dominance of exchange at high density, which is not included in our approximate CP potential. In practical terms, the blue electron is not "repulsive" enough. A more satisfactory solution can be obtained by performing a CP calculation in one spin channel only where the other spin CP density is fixed to that given by exchange alone. We turn to the details of this approach in the next section.

FIG. 4. Pair distribution function, $g(r)$ plotted vs r/r_s for $r_s = 0.02$. The dashed blue line is for the CP potential equal to $1/r$, the dotted red line is for the modified CP Potential, and the solid black line is the exact solution.

well-known for a uniform gas, given explicitly in Eq. (B2). In principle [13], the CP potential should now be two different potentials, one for each spin channel, and the functional dependence could differ for parallel and antiparallel spins. Here we simply use the same CP potential we have used for nonspin CP-DFT, [Eq. (6)]. For finite systems, using spin densities in CP-DFT is complicated, as in general they do not integrate up to integer particle numbers [13]. Here, this is not a concern, as the particle number is infinite. Moreover, in our calculation, we use the exchange pair correlation function, which does yield an integer particle number.

We consider a UEG with spin densities $\bar{n}_\uparrow$ and $\bar{n}_\downarrow$. Placing a *blue* $\uparrow$ electron at the origin, $r = 0$ and dropping the prime, it will be surrounded by its hole of $\uparrow$ electrons given by

$$\delta n_\uparrow(r) = \bar{n}_\uparrow [g_{\uparrow\uparrow}(\bar{n}_\uparrow, \bar{n}_\downarrow; r) - 1]. \qquad (11)$$

Here, $g_{\uparrow\uparrow}(\bar{n}_\uparrow, \bar{n}_\downarrow; r)$ is the PDF for like-spin electrons separated by a distance r in a uniform gas with given spin densities, $\bar{n}_\uparrow$ and $\bar{n}_\downarrow$. The up-spin density is then given by

$$\tilde{n}_\uparrow(r \uparrow) = \bar{n}_\uparrow + \delta n_\uparrow(r) = \bar{n}_\uparrow g_{\uparrow\uparrow}(\bar{n}_\uparrow, \bar{n}_\downarrow; r). \qquad (12)$$

With a known $\tilde{n}_\uparrow(r \uparrow)$, we can write down a KS equation for $\tilde{n}_\uparrow(r \downarrow)$ and solve for it within the local spin density approximation. Thus, *given* $g_{\uparrow\uparrow}$, we can calculate $g_{\uparrow\downarrow}$ via CP-DFT. As $g_{\uparrow\downarrow}$ contains no exchange, we can hope to be more accurate in the high density limit.

The numerical solution for the fixed spin case is carried out in a manner analogous to that for CP-DFT. Again, we consider two systems. First, the N- electron system with numbers of up and down spins, $N_\sigma = N/2$ and average spin densities, $\bar{n}_\sigma = N_\sigma/V$ and secondly, the $N - 1$ electron system with $N_\uparrow = N/2 - 1$ up spins and $N_\downarrow = N/2$ down spins. The N-electron system is initialized as $n(r \uparrow) = \bar{n}_\uparrow$, $n(r \downarrow) = \bar{n}_\downarrow$ and the $N - 1$ electron system is initialized as $\tilde{n}_\uparrow(r \uparrow) = \bar{n}_\uparrow g_x(\zeta, k_F r)$ and $\tilde{n}_\uparrow(r \downarrow) = \bar{n}_\downarrow$. Here, $\bar{n}_{\uparrow(\downarrow)}$ is understood as referencing the N or $N - 1$ electron system accordingly. Further details are contained in Appendix B. By using only g_x, which can be derived analytically, we avoid using any many-body results. For high densities, this will be extremely accurate.

In general, there are complications when using KS spin-DFT to find CP densities, because the individual components need not, in general, integrate to integer particle numbers. We explain this in a forthcoming paper on the formalism, in general [13]. However, such issues do not apply for a uniform gas, which is why we use spins here. But it is also why we do not pursue this as a general strategy: It is too complicated to use in inhomogeneous cases. See the discussion following Eq. (10) of the current paper.

D. Computational details

Calculations can be carried out on personal computers, typically lasting minutes or hours. Our model was written in Python 3 utilizing NumPy [23], SciPy [24], Numba [25], and an exchange-correlation module "excor.py" written by K. Haule (Physics Dept. Rutgers University).
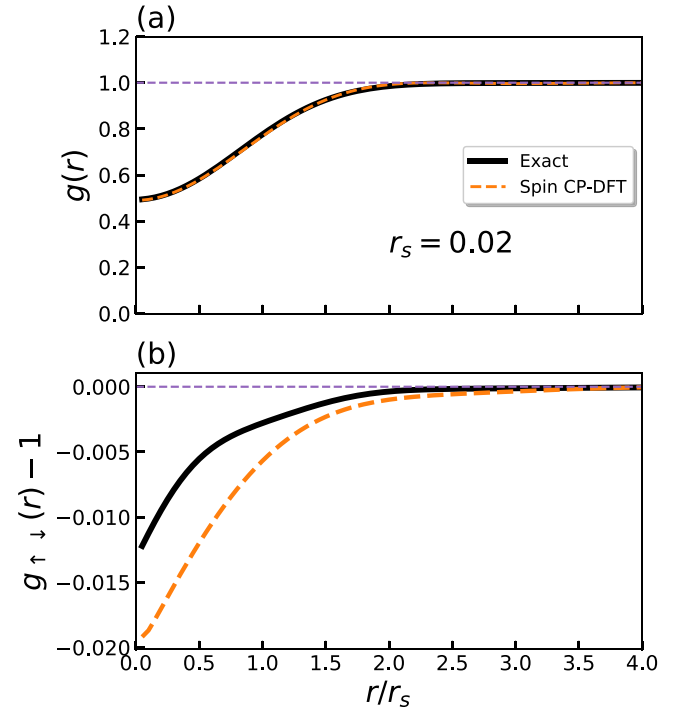

FIG. 5. Pair distribution function (a) and antiparallel PDF-1 (b) vs r/r_s for the spin CP-DFT with $r_s = 0.02$. Solid black line is the exact result and the orange dotted line is the spin CP-DFT.

E. Spin CP-DFT results

The calculations for the spin CP-DFT use the modified version of the CP potential Eq. (9b). Additionally we are setting the correlation potential to zero. We had also performed calculations using the correlation potential but found that for densities $r_s \lesssim 7.5$ the results were worse compared to setting the correlation potential to zero. For lower densities, including the correlation potential gave better results but since our goal is to remedy the failure of CP-DFT in the high density regime, we chose to set the correlation potential to zero. We first consider an electron density of $r_s = 0.02$. We plot the result for the PDF in Fig. 5. The agreement is excellent as at such a high density the interactions are dominated by exchange. We also plot $g_{\uparrow\downarrow}(r)$ in Fig. 5 and these results are also quite good.

We next consider a lower density of $r_s = 2.5$. We show results for the total PDF in Fig. 6(a) and for the antiparallel PDF in Fig. 6(b). Although there is some small difference with the exact result for the antiparallel PDF, the overall PDF is good and the error in potential XC energy is about 3%.

We see a more serious departure from the exact result at $r_s = 10.0$. Figures 7(a) and 7(b) plot the PDF and antiparallel PDF for this low density. Here we can see more clearly the departure from the exact result although the relative error for the potential XC energy is on the same order as that for $r_s = 2.5$ but with the sign reversed.

In Fig. 8 we plot the potential XC energy times r_s as a function of r_s for both models. The agreement with the exact result is quite good for the spin CP-DFT, being worst at low density.

Since, as noted above, for values of $r_s \gtrsim 2.5$, the fractional error for the CP-DFT is on the order of 3%, the question
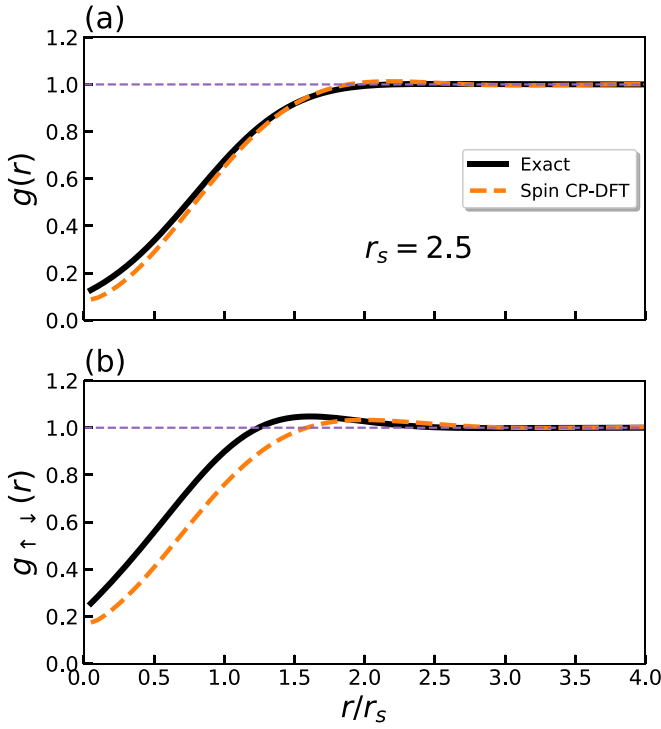
FIG. 6. Same as for Fig. 5 but for $r_s = 2.5$.

arises as to whether an additional potential can be added to the CP-DFT to correct for its deficiencies at high density. In fact, such an additional potential was used in our previous work [11], where we found that an added, external potential of
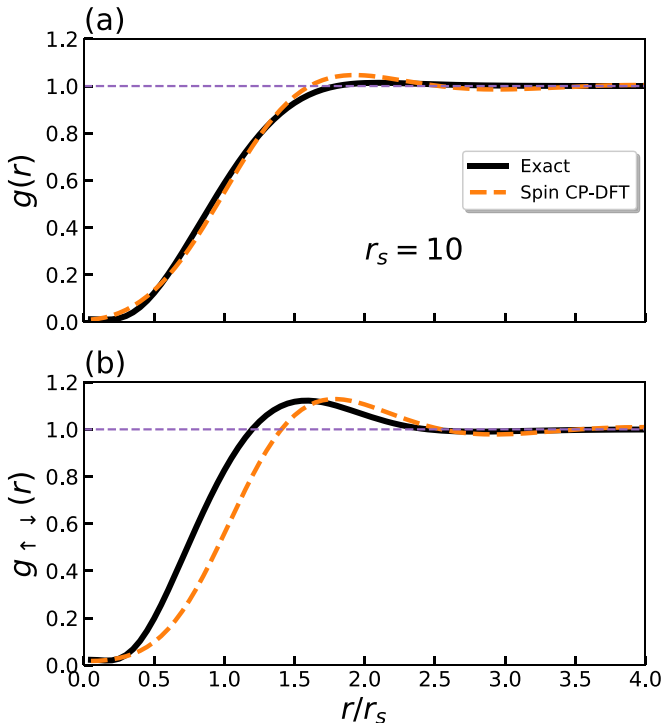
FIG. 7. Same as for Fig. 5 but for $r_s = 10.0$.
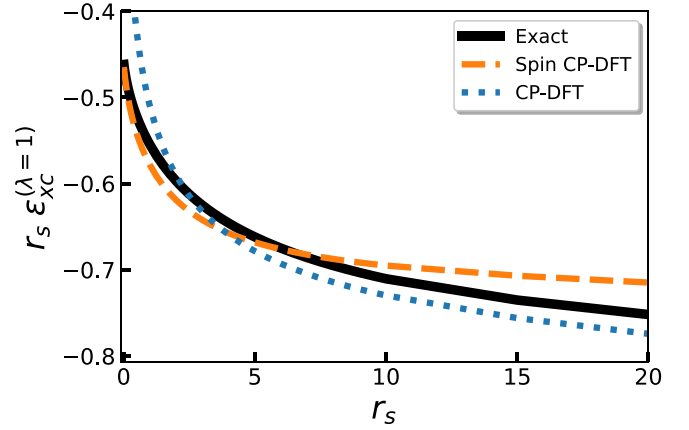
FIG. 8. $r_s \varepsilon_{\text{XC}}^{(\lambda=1)}$ vs r_s. The solid black line is the exact result, the dotted orange line is the spin CP-DFT, and the dotted blue line is for the CP-DFT.

Gaussian shape

$$v_G(r) = A(r_s)e^{-r^2/2\sigma^2(r_s)}, \tag{13}$$

where $A(r_s)$ and $\sigma(r_s)$ are r_s-dependent strength and range parameters provides the needed repulsive effect. The r_s dependence was chosen to replicate exchange in the high density limit, and to slowly turn off as r_s grows, vanishing beyond $r_s = 2.5$. This is described in Appendix C. The results of using the Gaussian potential, Eq. (13) with the strength and range parameters given by Eq. (C3) are shown in Fig. 9 where the maximum difference with the exact result for the two-channel model is now less than 3%. This was used in Ref. [11].

The coupling-constant averaged values of the XC energy, ε_{xc}, can be obtained by calculating the potential XC energy, $\varepsilon_{xc}^{(\lambda)}$, Eq. (A15), with $\lambda = 1$ for a series of r_s values and integrating over r_s [19]

$$\varepsilon_{\text{XC}}(r_s) = \frac{1}{r_s^2} \int_0^{r_s} r_s' \varepsilon_{\text{XC}}^{\lambda=1}(r_s')dr_s'. \tag{14}$$

The comparison with PW92 for the XC energy is shown in Fig. 10 where the relative difference is below 4% for the single
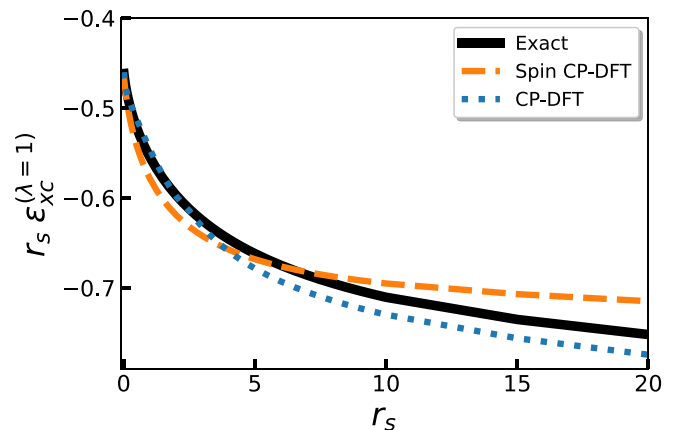

FIG. 9. Same as for Fig. 8 but where the CP-DFT has the added Gaussian potential.
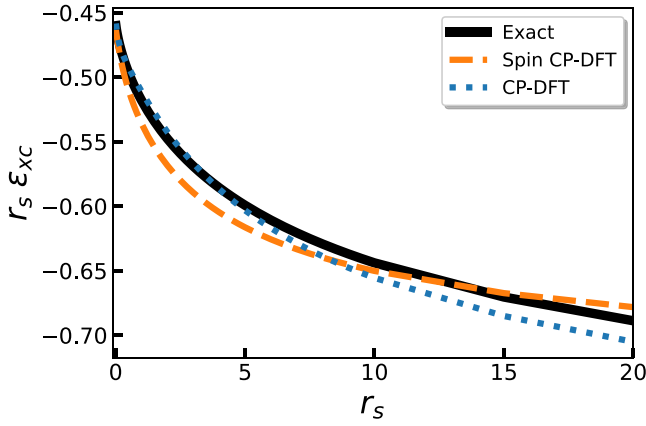
FIG. 10. Coupling-constant averaged exchange-correlation energies plotted as $r_s \varepsilon_{xc}$ vs r_s. The solid black line is the exact result, the dashed orange line is for the spin CP-DFT, and the dotted blue line is for the CP-DFT with the added Gaussian potential.

channel model and for the two-channel model with Gaussian repulsion is below 3%.

IV. THOMAS-FERMI SOLUTION FOR THE BLUE ELECTRON PROBLEM

The Thomas-Fermi functional [26,27] for the blue electron system is

$$F^{TF}[n] = \int d^3 r \left[A_s n^{5/3}(\mathbf{r}) + v_{\mathrm{n}}(\mathbf{r}) n(\mathbf{r}) \right.$$
$$\left. + \frac{1}{2} v_{\mathrm{H}}(\mathbf{r}) n(\mathbf{r}) + \Delta \tilde{v}(\mathbf{r}) n(\mathbf{r}) \right] \qquad (15)$$

with $A_s = (3/10)(3\pi^2)^{2/3}$. The potentials, v_{n}, Eq. (A2) and v_{H}, Eq. (8) are as before and we use $\Delta \tilde{v}(r) = 1/r$. The charge densities are normalized such that $\int d^3 r \, n_0 = N$ and $\int d^3 r \, n(\mathbf{r}) = N - 1$.

Defining the total electrostatic potential as $V(\mathbf{r}) = v_{\mathrm{n}}(\mathbf{r}) + v_{\mathrm{H}}(\mathbf{r}) + \Delta \tilde{v}(\mathbf{r})$ minimizing the functional, Eq. (15) with respect to the density, $n(\mathbf{r})$ subject to the normalization condition, and formally solving for the density, we have (just as for bare atoms or ions):

$$n(\mathbf{r}) = \left(\tfrac{5}{3} A_s \right)^{-3/2} [\mu - V(\mathbf{r})]_+^{3/2}, \qquad (16)$$

where $x_+ = 0$ if $x < 0$ and μ is the chemical potential.

As $r \to \infty$, $n(r) \to n_0$, and thus $V(r) \to 0$. The latter can be determined from a Taylor expansion of the denominator in $V(\mathbf{r})$. From Eq. (16), we find

$$\mu = \tfrac{5}{3} A_s n_0^{2/3}. \qquad (17)$$

But as $r \to 0$, $V \sim 1/r$, so $\mu - V \to -\infty$. Thus, $\mu = V$ at some r_0, so $n = 0$ for $r \leqslant r_0$ in Eq. (16).

We relate the Laplacian of the electrostatic potential to the charge densities using Poisson's equation

$$\nabla^2 V((\mathbf{r})) = -4\pi [n(\mathbf{r}) - n_0 + \delta(\mathbf{r})]. \qquad (18)$$

Defining

$$\frac{\phi(r)}{r} = \mu - V(r) \qquad (19)$$

and $\delta\phi(r) = \phi(r) - \mu r = -rV(r)$ and substituting from Eq. (16) we have

$$\nabla^2 \left(\frac{\delta\phi}{r} \right) = 4\pi \left[-n_0 + \left(\frac{5}{3} A_s \right)^{-3/2} \left(\frac{\delta\phi}{r} \right)^{3/2} \Theta(r - r_0) \right], \qquad (20)$$

where $\Theta(x)$ is a step function in x, and the δ function at $r = 0$ implies:

$$\delta\phi(0) = -1, \quad \delta\phi(r_0) = -\mu r_0. \qquad (21)$$

Introducing dimensionless variables $z = r/r_s$ and $y = \delta\phi/\mu r_s$ we can write Eq. (20) as

$$\frac{d^2 y}{dz^2} = x_s z \left(-1 + \left(1 + \frac{y}{z} \right)_+^{3/2} \right), \qquad (22)$$

with $x_s = r_s/a$, and $a = (3\pi^2/16)^{1/3}/2 \approx 0.61$. The boundary conditions are

$$y(0) = -\frac{x_s}{3}, \quad y(z_0) = -z_0, \quad y \to 0 \text{ as } z \to \infty, \qquad (23)$$

where $z_0 = r_0/r_s$. For $z < z_0$,

$$y(z) = -\left(\frac{x_s}{2} \right) z^3 + Az + B, \qquad (24)$$

where

$$A = \left(\frac{x_s}{3z_0} \right) \left[1 + \frac{z_0^3}{2} \right] - 1, \quad B = -\frac{x_s}{3}. \qquad (25)$$

For $z > z_0$, we have, for large z, to first order

$$\frac{d^2 y}{dz^2} \approx 3x_s \frac{y}{2}, \qquad (26)$$

yielding $y(z) \propto e^{-kz}$ where $k = (3x_s/2)^{1/2}$. By matching the log derivatives at $z = z_0$ between Eq. (24) and the large z solution, at $z = z_0$, we find

$$z_0^3 + \frac{3k}{x_s} z_0^2 + \frac{3}{x_s} z_0 - 1 = 0. \qquad (27)$$

The solution to Eq. (27) depends on the value of r_s. For $r_s < a/\sqrt[3]{2} \approx 0.4872$, there are three real roots but only 1 is positive and for larger r_s there is only 1 real root. Thus,

$$z_0 = \begin{cases} Q^{1/2} \left[2\cos\left(\frac{\theta + \pi}{3} \right) + \sqrt{3} \right] & r_s < a/\sqrt[3]{2} \\ A + Q/A - \sqrt{3}Q & r_s > a/\sqrt[3]{2}, \end{cases} \qquad (28)$$

where $\theta = \cos^{-1}(\sqrt{2x_s^3})$, $Q = 1/2x_s$, and $A = [1/2 + (1/4 - Q^3)^{1/2}]^{1/3}$. The numerical solution to the TF blue electron model is detailed in Appendix D.

We performed calculations for r_s values ranging from $r_s = 0.02$ to $r_s = 100$. Plots of the normalized hole densities for these r_s values are shown in Fig. 11. As can be seen in this figure, the normalized hole density tends toward a step function at $r = r_s$ in the low density limit and the location of z_0 moves farther out. In Fig. 12 we plot the value of z_0 as a function of r_s as determined from the numerical calculations, as well as the analytic approximation of Eq. (28). The analytic
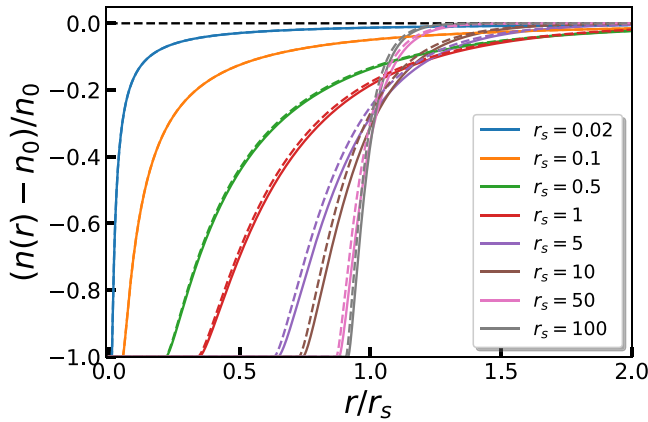
FIG. 11. Normalized hole density vs r/r_s for a range of densities. Solid lines are the numerical solutions and the dashed lines are for the analytic solutions.

solution for z_0 is surprisingly accurate with a maximum error of 2.3% around $r_s = 5.0$. A table of values for the numerical and analytical results for z_0 can be found in Table I.

We can calculate the potential XC energy from the CP hole density, $n_{xc}(r) = n(r) - n_0$ using Eq. (A15). In Fig. 13 we plot potential energy $r_s \varepsilon_{xc}^{(\lambda=1)}$ and compare with the exact result as well as the KS blue electron result using CP-DFT with $\Delta \tilde{v}(r) = 1/r$. We also plot the fractional error in Fig. 14. For mid- to low densities ($r_s \geqslant 1.0$) the results are surprisingly good, with errors less than 10%. It is instructive at this point to plot the PDF vs r/r_s for different values of r_s and compare with the exact result. This comparison is shown in Fig. 15 for $r_s = 0.02, 1.0, 5.0, 10.0$. The results are poor at $r_s = 0.02$ but improve with decreasing density. Interestingly enough, although the shape of the hole is inaccurate at $r_s = 1.0$, the integrated value of the hole energy is quite good when compared to the exact result.

V. CONCLUSIONS

We have shown how to implement the blue-electron concept for a uniform gas at low temperature. The simple classical
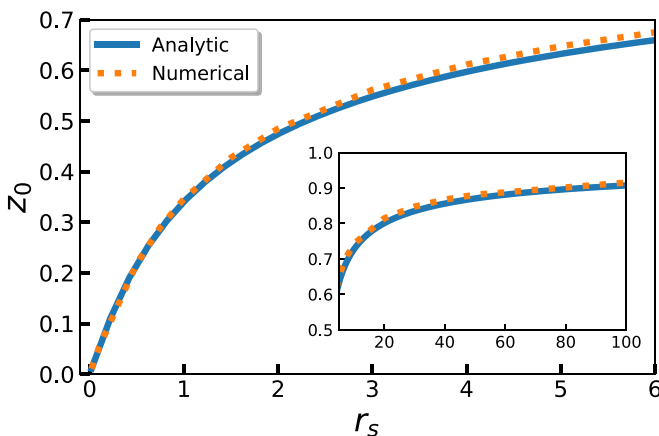
TABLE I. Values of z_0 as a function of r_s analytic and exact calculations along with the relative error between them.

r_s	z_0^A	z_0	$(z_0^A - z_0)/|z_0|$
0.02	0.0108	0.0108	−0.0000
0.1	0.0529	0.0529	−0.0004
0.5	0.2168	0.2186	−0.0081
1.0	0.3404	0.3460	−0.0161
5.0	0.6322	0.6472	−0.0233
10.0	0.7272	0.7425	−0.0205
50.0	0.8704	0.8809	−0.0119
100.	0.9071	0.9153	−0.0089

idea of an impurity captures the basic physics for moderate to low densities, and its accuracy is improved by a local density approximation for the CP potential that respects the electron-electron cusp condition at short distances.

The blue-electron idea naturally fails at high densities, where exchange effects dominate. We have shown how this failure can be overcome by applying the idea for anti-parallel spin alone, while using just the exchange hole for parallel spin. Our procedure still avoids any many-body or QMC input, and provides useful accuracy for all densities, including the high-density limit. Moreover, it provides formal justification for the large Gaussian repulsion used when the entire hole is simulated for high-densities, and its smooth turning off. Errors no greater than 5% in the XC energy density are then available.

As the method is based on classical DFT ideas, we expect errors to lessen with increasing temperature, and overall, they do [11]. But we have also given results for TF blue electron calculations, as higher-temperature simulations often must use TF in place of KS because of convergence issues with the KS scheme. Here we present our analysis of the TF equation just at zero temperature. A simple analytic approximation is remarkably accurate relative to a fully converged numerical solution. We use the numerical solution to compare with KS blue electron calculations at zero temperature. Again, we expect the error introduced by the TF approximation to reduce with increasing temperature.

FIG. 12. Value of z_0 vs r_s. The solid line is derived from Eq. (27) and the dotted line is from the numerical calculations.
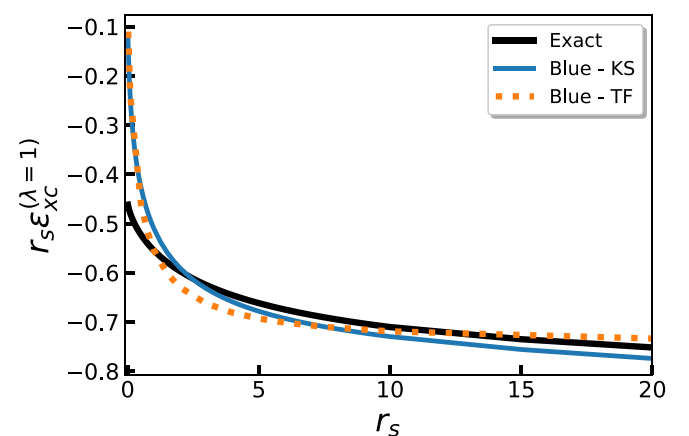

FIG. 13. $r_s \varepsilon_{xc}^{(\lambda=1)}$ vs r_s for the TF blue electron model, the KS blue electron model, and the exact result.
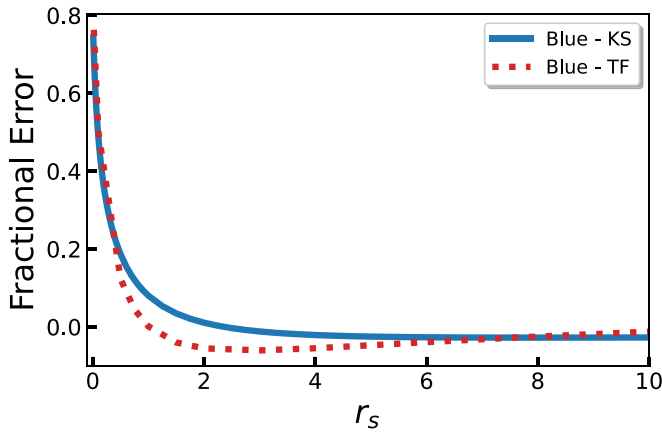
FIG. 14. Fractional error for the TF model), KS model, and the exact result. The comparisons are with the noncoupling-constant averaged energies.

Even at low temperature, where convergence of KS is not an issue, the TF blue electron might prove a pragmatic alternative to full CP-DFT calculations, as these require a KS calculation at every point in the system.

Regardless of the accuracy of these specific calculations, the principle that one could calculate XC holes and their energies exactly via the densities of many KS calculations remains valid. Moreover, the CP approach provides a useful bypass of the need to find more accurate XC functionals, albeit at higher computational cost. It remains to be seen whether
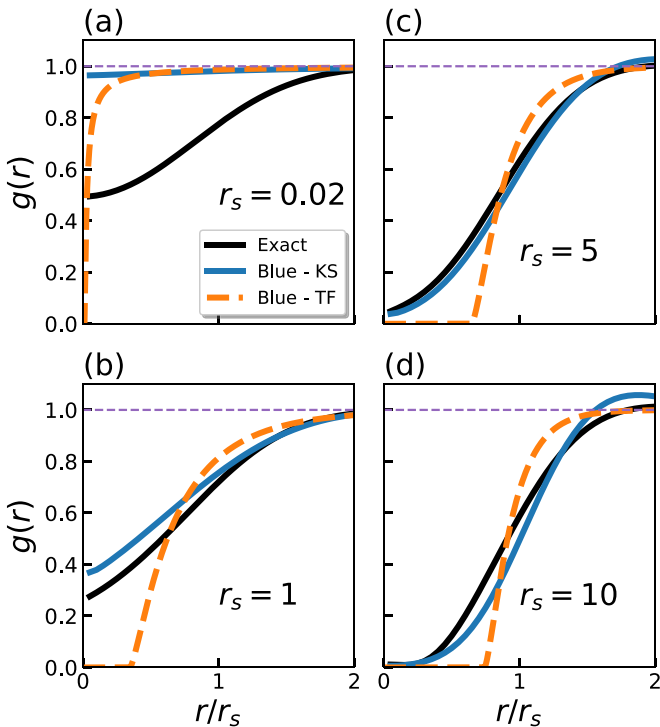

FIG. 15. PDF vs r/r_s for (a) $r_s = 0.02$, (b) $r_s = 1.0$, (c) $r_s = 5.0$, (d) $r_s = 10.0$ The solid black line is the exact result, the solid blue line is the CP-DFT with $\Delta \tilde{v} = 1/r$, and the dashed orange line is the Thomas-Fermi model.

CP-DFT can evolve into a practical alternative to existing DFT calculations, especially in situations where standard DFT fails.

APPENDIX A: CP-DFT DETAILS

Here we provide further details of the CP-DFT and our method of numerical solution. In addition to the Hartree, Eq. (8) and CP potentials Eq. (9) used in the KS equations, Eq. (7), we have the exchange interaction in the LDA,

$$v_{\text{X}}^{\text{LDA}}[n](r) = \left(\frac{3}{2\pi}\right)^{2/3} \frac{1}{r_s[n(r)]}, \quad (A1)$$

and, when used, the correlation potential, $v_{\text{C}}[n](r)$ is from PW92. The positive, compensating background potential is

$$v_{\text{n}}(\mathbf{r}) = -\int d^3 r' \frac{n_0}{|\mathbf{r} - \mathbf{r}'|} = -4\pi \bar{n}\left(\frac{R^2}{2} - \frac{r^2}{6}\right). \quad (A2)$$

Our system is spherically symmetric, hence we can write the wave functions in terms of spherical harmonics and a radial wave function,

$$\phi_i(\mathbf{r}) = R_{nl}(r) Y_{lm}(\theta, \phi) = \frac{u_{nl}(r)}{r} Y_{lm}(\theta, \phi), \quad (A3)$$

with quantum numbers n, l, m and we have expressed the radial wave function as $u(r)/r$. The radial KS equation is

$$\left[-\frac{1}{2}\frac{d^2}{dr^2} + v_{\text{s}}(r) + \frac{l(l+1)}{2r^2}\right] u_{nl}(r) = \varepsilon_{nl} u_{nl}(r). \quad (A4)$$

The density is

$$n(r) = 2 \sum_{n,l} \frac{2l+1}{4\pi} \frac{u_{nl}^2(r)}{r^2} f((\varepsilon_{nl} - \mu)/k_B T), \quad (A5)$$

where the factor of 2 accounts for spin and $f((\varepsilon_{nl} - \mu)/k_B T)$ is the Fermi-Dirac distribution function used for Fermi *smearing* of the energy states,

$$f(x) = (1 + e^x)^{-1}. \quad (A6)$$

Here, μ is the chemical potential chosen so that

$$N = 2 \sum_{n,l} (2l+1) f((\varepsilon_{nl} - \mu)/k_B T), \quad (A7)$$

where N is the number electrons and $k_B T$ is Boltzmann's constant times the temperature. Smearing reduces convergence issues. All calculations use $\phi = 0.05$ defined as

$$\phi = \frac{k_b T}{\varepsilon_F^{ni}}, \quad (A8)$$

where ε_F^{ni} is the Fermi energy for the noninteracting electron gas

$$\varepsilon_F^{ni} = \frac{1}{2}\left(\frac{9\pi}{4}\right)^{2/3} r_s^{-2}. \qquad (A9)$$

The set of equations describing the CP-DFT are coupled and thus have to be solved self-consistently. We do this using an iterative scheme wherein first, an initial guess is made for the density, $n(r)$. Then, the KS equations are solved using that initial guess and a new density, $n^*(r)$ evaluated from Eq. (A5). This density is then mixed in with the previous density via linear mixing:

$$n^{k+1}(r) = \alpha n^*(r) + (1 - \alpha)n^k(r), \qquad (A10)$$

where k represents the kth iteration and $\alpha < 1$. This process is repeated until a suitable convergence to be described below is obtained. We use a shooting method to solve for the wave function that satisfies Eq. (A4) for a given energy, ε_{nl}. A 4th order Runge-Kutta scheme is used to integrate Eq. (A4) forward from $r = r_0$ to $r = R$ with typical values $r_0 = 0.05r_s$ and $R = 8r_s$, respectively. Following Ref. [28] the boundary condition used at $r = r_0$ is

$$u_{nl}(r = r_0) = Ar_0^{l+1}$$
$$\left.\frac{du}{dr}\right|_{r=r_0} = A(l+1)r_0^l, \qquad (A11)$$

where A is some constant. For the boundary condition at $r = R$, we require $\partial n(r)/\partial r|_{r=R} = 0$. To ensure this we require

$$\left.\left(\frac{\partial u(r)}{\partial r} - \frac{u(r)}{r}\right)\right|_{r=R} = 0. \qquad (A12)$$

Solving the KS equations for a specific l involves varying the energy ε in small increments, integrating Eq. (A4) for each value of the energy and looking for regions where Eq. (A12) changes sign. A root-finding scheme is then used to precisely locate the energy eigenvalue.

We use two criteria for convergence of the iterative solution scheme. The first is that the difference of the sum over all states of the energy eigenvalues between the new state before mixing and the previous iteration relative to the new state must be less than 5×10^{-7}. The second is that the 2-norm of the density difference between successive iterations normalized by the 2-norm of the density is less than 10^{-5}. Both criteria must be satisfied for convergence.

The procedure for a blue electron calculation is then to solve both the N electron system with $\Delta\tilde{v} = 0$ and the $N - 1$ electron system with $\Delta\tilde{v}$ as in Eq. (9) for a given system density. With the densities obtained from these two calculations, $n(r)$ and $\tilde{n}(r)$, we calculate the XC hole density as

$$n_{\text{XC}}^{\lambda=1}(r) = \tilde{n}(r) - n(r) \qquad (A13)$$

and from the hole density obtain the PDF

$$g(r) = \frac{n_{\text{XC}}^{\lambda=1}(r)}{\bar{n}} + 1. \qquad (A14)$$

The XC energy can be calculated as

$$\varepsilon_{\text{XC}}^{(\lambda)} = 2\pi \int_0^R r\, n_{\text{XC}}^{(\lambda)}(r)dr. \qquad (A15)$$

APPENDIX B: SPIN CP-DFT DETAILS

The spin CP-DFT considers the up-spin density fixed by Eq. (12) and solves for the down spin density, $n_\uparrow(r\downarrow)$. Thus we need an expression for the like-spin PDF. An analytic fit to the like-spin PDF can be obtained from Eq. (48) of PW92

$$g_{\uparrow\uparrow}(r_s, \zeta, k_F r) = g[r_s, 1, (1+\zeta)^{1/3}k_F r/2^{1/3}], \qquad (B1)$$

where $r_s = (3/4\pi\bar{n})^{1/3}$ is the Wigner-Seitz radius, $\bar{n} = \bar{n}_\uparrow + \bar{n}_\downarrow$, $k_F = (3\pi^2\bar{n})^{1/3}$ is the Fermi wave vector, $\zeta = (\bar{n}_\uparrow - \bar{n}_\downarrow)/(\bar{n}_\uparrow + \bar{n}_\downarrow)$ is the spin polarization. In our calculations, we include only the exchange part of the like-spin PDF

$$g_{\text{x}}(\zeta, k_F r) = 1 + \frac{1}{2}\sum_{\sigma=-1}^{+1}(1+\sigma\zeta)^2 J[(1+\sigma\zeta)^{1/3}k_F r], \qquad (B2)$$

where

$$J(y) = -\frac{9}{2}\frac{j_1(y)}{y} \qquad (B3)$$

and j_1 is the spherical Bessel function of the first kind. Similar to the neutral spin case, we can write the KS orbitals for $n_\downarrow(r)$ in terms of spherical harmonics and a radial function. This leads to a KS equation for $n_\downarrow(r)$ similar to Eq. (A4) but without the 2 for spin degeneracy.

The KS potential is as before but now the exchange potential is

$$v_{\text{x},\sigma}^{LDA}[n, \zeta](r) = \frac{4}{3}\varepsilon_x(n, \zeta) - \frac{2}{3}(\zeta - \text{sgn}(\sigma))\varepsilon_{\text{x}}^{\text{unpol}}(n)$$
$$\times \{(1+\zeta)^{1/3} - (1-\zeta)^{1/3}\}. \qquad (B4)$$

Here, $\text{sign}(\sigma) = \pm 1$ as $\sigma = \uparrow$ or $\sigma = \downarrow$. The unpolarized exchange energy is

$$\varepsilon_{\text{x}}^{\text{unpol}}(n) = -\frac{3}{4}\left(\frac{3}{\pi}\right)^{1/3} n^{1/3}, \qquad (B5)$$

and the polarized exchange energy is

$$\varepsilon_{\text{x}}(n, \zeta) = \varepsilon_{\text{x}}^{\text{unpol}}(n)\left\{\frac{(1+\zeta)^{4/3} + (1-\zeta)^{4/3}}{2}\right\}. \qquad (B6)$$

Note that in the above equations, $\zeta = \zeta(r)$ is the local spin polarization. The correlation potential, when used, is from PW92 and the CP potential is as before.

The $n_\uparrow(r)$ is kept fixed and the KS equations are solved for the down spin density in a manner analogous to that of the CP-DFT case. Once the down spin densities are obtained, the PDF can be calculated as before using Eq. (A13) and Eq. (A14). Additionally we can calculate the antiparallel PDF from

$$g_{\uparrow\downarrow}(r) = \frac{n_{\text{XC},\downarrow}(r)}{\bar{n}_\downarrow} + 1, \qquad (B7)$$

with

$$n_{\text{XC},\downarrow}^{(\lambda=1)}(r) = \tilde{n}_\uparrow(r\downarrow) - n(r\downarrow). \qquad (B8)$$

APPENDIX C: DETERMINATION OF PARAMETERS FOR THE GAUSSIAN POTENTIAL

The parameters for this added potential were obtained by varying values of A and σ in a grid search and evaluating two
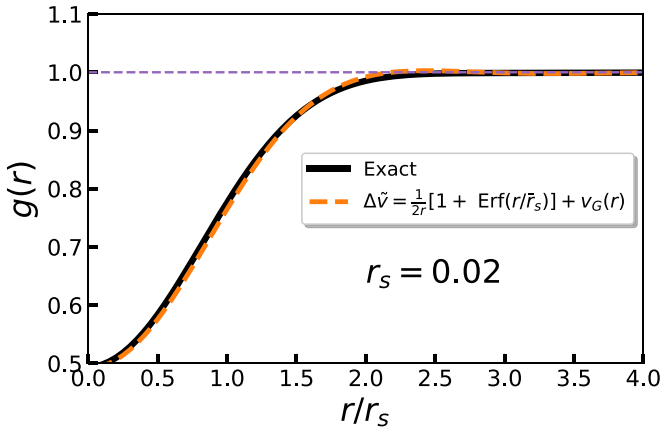
FIG. 16. Pair distribution function, $g(r)$ plotted vs r/r_s for $r_s = 0.02$. The solid black line is the exact PDF and the dashed orange line is for the modified CP potential plus the added Gaussian of Eq. (13).

metrics. The first is the relative difference with PW92 for the on-top hole density at $r = 0$, i.e.,

$$M_A = \frac{(n_{xc}(r \to 0) - n_{xc}^{PW}(r \to 0))}{|n_{xc}^{PW}(r \to 0)|} \quad \text{(C1)}$$

and the second is the relative difference with the PW92 exchange-correlation energy,

$$M_B = \frac{(\varepsilon_{xc} - \varepsilon_{xc}^{PW})}{|\varepsilon_{xc}^{PW}|}. \quad \text{(C2)}$$

The zero contours from the grid search of each of these metrics was calculated and the values for A and σ determined from the intersection of these zero contours. The results at $r_s = 0.02$ were $A = 2322.2065$ and $\sigma = 0.01145$. Using these values in Eq. (13) matches the PW92 PDF for $r_s = 0.02$ very well as can be seen in Fig. 16.

The behavior of A and σ as determined by additional grid searches appeared to have power-law dependences, at least in the region of high densities (low r_s). However, this held true only for a very narrow range of r_s values and quickly departed from this behavior as r_s increased. We decided that the parameters of the Gaussian potential would have this power-law behavior but would be multiplied by a switching function such that by the time $r_s = 2.5$ was reached, the Gaussian potential parameters vanished. Thus, we used the following:

$$\begin{aligned} A(r_s) &= A_0 f_s(r_s, r_R, b_A)/r_s^2, \\ \gamma(r_s) &= \gamma_0 f_s(r_s, r_R, b_G)/r_s, \end{aligned} \quad \text{(C3)}$$

where

$$\sigma(r_s) = \frac{1}{\gamma(r_s)} \quad \text{(C4)}$$

and the switching function, f_s is given by [29]

$$f_s(r, r_R, b) = \begin{cases} \frac{1}{1-e^{-b}}\left(e^{-b\left(\frac{r}{r_R}\right)} - e^{-b}\right) & 0 \leqslant r \leqslant r_R \\ 0 & r_R \leqslant r. \end{cases} \quad \text{(C5)}$$

Here, r_R denotes the range over which the switching function goes from one to zero and b is a parameter controlling the shape of the switch. In the limit of $b \to 0$, the switch is a

linear function. The utility of this function is the wide range of switching behaviors that it can display, from rapid decrease and subsequent slower decline to slow decline followed by rapid decrease and as mentioned above, a simple linear decline.

The procedure we applied to determine the parameters was as follows. We would choose a set of parameters for the switching functions, i.e., b_A, b_γ (Note that we use the same r_R parameter for both A and γ but allow for different $b_{A(\gamma)}$ values.) The value for r_R was set to $r_s = 2.5$. The parameters A_0 and γ_0 are determined from the values obtained from the grid search at $r_s = 0.02$,

$$\begin{aligned} A_0 &= \frac{A(r_s = 0.02)(0.02)^2}{f_s(0.02, r_R, b_A)}, \\ \gamma_0 &= \frac{\gamma(r_s = 0.02)(0.02)}{f_s(0.02, r_R, b_\gamma)}. \end{aligned} \quad \text{(C6)}$$

Then, b_A and b_γ are varied until there is a smooth to the eye transition from the $r_s = 0.02$ value to the $r_s = 2.5$ value when plotting $r_s\varepsilon_{xc}$ vs r_s. The values of $r_R = 2.5$, $b_A = 3.0$, $b_\gamma = -3.0$ appeared to work best.

APPENDIX D: NUMERICAL METHOD FOR THE THOMAS-FERMI BLUE ELECTRON MODEL

As discussed above, we only expect Eq. (27) to be valid at high densities. Nonetheless, it can used to get an initial approximation for z_0 at all densities. Using the solution to Eq. (27) as an initial guess for z_0, we can numerically integrate Eq. (22) starting from $z = 0$ with the boundary conditions Eq. (23). We continue the numerical integration until certain criteria are reached. First, it may occur that $y(z) > 0$. In this case, our initial guess for z_0 is too low and needs to be increased. Second, it may occur that $dy(z)/dz < 0$. In this case, the solution is tending away from zero which is where the solution must go as $z \to \infty$. Here, z_0 must be decreased. Lastly, we may find that $d \ln(y)/dz = -k$ to within some designated tolerance. This means that we have effectively reached the large z region of Eq. (22) for the particular value of r_s being used and we can now switch to the analytic result to obtain the solution for larger z values. Once Eq. (22) has been integrated to a point, $z = z_{ldm}$ where the log-derivative matches $-k$ to the specified tolerance, the value of the constant, A_0 can be determined from

$$A_0 = y(z_{ldm})e^{kz_{ldm}}. \quad \text{(D1)}$$

We used a fourth-order Runge-Kutta scheme with a step size of 10^{-5} to integrate Eq. (22). Initial work showed that the value of z_0 obtained from Eq. (27) is slightly below that of the actual value and so we created a bracket with the lower guess, z_0^L from Eq. (27) and the upper guess being $z_0^R = z_0 + 0.1$. We then solve Eq. (22) using $z_0 = (z_0^L + z_0^R)/2$ until one of the above stopping criteria are reached. If the log-derivative matches to that of $-k$ with a tolerance of 1.0×10^{-8}, then we have found z_0. If, one of the other criteria is reached, we adjust either the lower or upper guess and repeat the process until the log-derivative is matched. This iterative process required some 10–50 iterations depending on the density. The numerical solution to Eq. (22) for $r_s = 1.0$ with the value
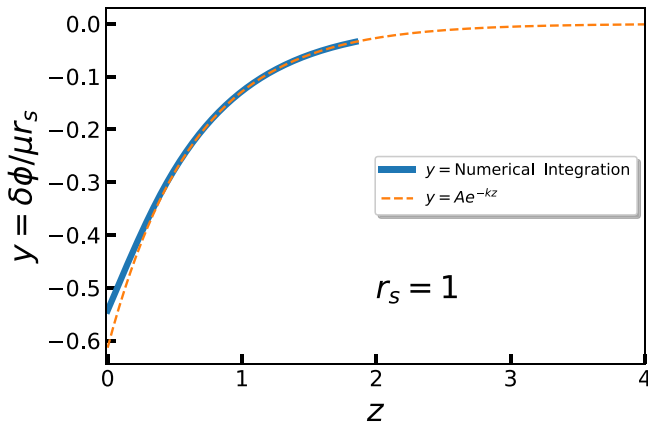
FIG. 17. The solution to Eq. (22) for $r_s = 1.0$. The solid line is the numerical solution and the dashed line is the large z solution with the value of A_0 given by Eq. (D1).

FIG. 18. Normalized hole density vs r/r_s for $r_s = 1.0$ Solid line is the result from the numerical calculation whereas the orange dashed line is from the exponential solution with A_0 determined from Eq. (D1) while the dashed green line is the analytic solution with A_0 determined by the boundary conditions. The inset shows the region for $r_s \lesssim 0.5$.

of $z_0 = 0.3460$ found by the iterative process is shown in Fig. 17 along with the exponential solution with A_0 obtained from Eq. (D1) The normalized hole density, $(n(r) - n_0)/n_0$ for the case of $r_s = 1.0$ is shown in Fig. 18 along with the exponential solution with A_0 obtained from Eq. (D1) and an analytic solution where A_0 is obtained from the boundary conditions, Eq. (23) using the z_0 value obtained from Eq. (27). A closer look at the region for $r/r_s < 0.5$ is shown in the inset where we can see the differences between the numerical solution and the exponential and purely analytic solutions. As a last check on the calculation, we can calculate the integral
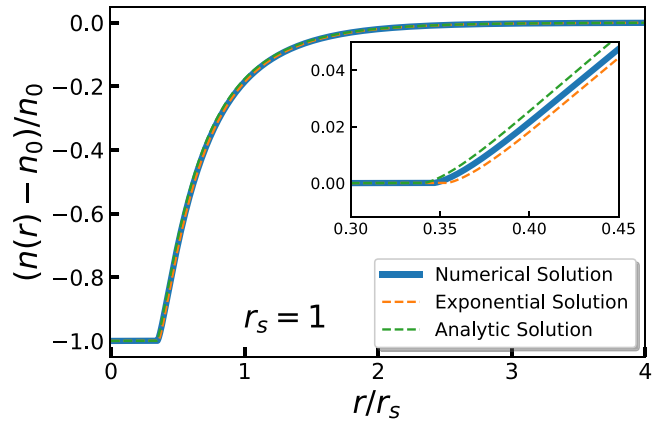
of the hole density for the different solutions and it should integrate to -1. The numerical and exponential solutions satisfies this condition to about 0.04% and 0.40%, respectively, whereas the purely analytic solution is off by approximately 5%. We note that for matching the log derivatives, a tolerance of 10^{-8} is necessary to have the hole density integrate to -1. At lower densities, a lower tolerance of 10^{-6} works just fine.

[1] G. F. Giuliani and G. Vignale (eds.), *Quantum Theory of the Electron Liquid* (Cambridge University Press, Cambridge, 2008).
[2] R. Jones and O. Gunnarsson, Rev. Mod. Phys. **61**, 689 (1989).
[3] K. Burke, J. Chem. Phys. **136**, 150901 (2012).
[4] D. M. Ceperley and B. J. Alder, Phys. Rev. Lett. **45**, 566 (1980).
[5] S. H. Vosko, L. Wilk, and M. Nusair, Can. J. Phys. **58**, 1200 (1980).
[6] J. P. Perdew and A. Zunger, Phys. Rev. B **23**, 5048 (1981).
[7] J. P. Perdew and Y. Wang, Phys. Rev. B **45**, 13244 (1992).
[8] V. V. Karasiev, T. Sjostrom, J. Dufty, and S. B. Trickey, Phys. Rev. Lett. **112**, 076403 (2014).
[9] S. Groth, T. Dornheim, T. Sjostrom, F. D. Malone, W. M. C. Foulkes, and M. Bonitz, Phys. Rev. Lett. **119**, 135001 (2017).
[10] T. Dornheim, A. Cangi, K. Ramakrishna, M. Böhme, S. Tanaka, and J. Vorberger, Phys. Rev. Lett. **125**, 235001 (2020).
[11] R. J. McCarty, D. Perchak, R. Pederson, R. Evans, Y. Qiu, S. R. White, and K. Burke, Phys. Rev. Lett. **125**, 266401 (2020).
[12] P. Mori-Sánchez, A. J. Cohen, and W. Yang, Phys. Rev. Lett. **100**, 146401 (2008).
[13] R. Pederson, J. Chen, S. R. White, and K. Burke, Conditional probability density functional theory, arXiv:2203.09647.
[14] P. A. M. Dirac, Math. Proc. Cambridge Philos. Soc. **26**, 376 (1930).
[15] J. Chihara, J. Phys.: Condens. Matter **3**, 8715 (1991).
[16] M.-C. Kim, E. Sim, and K. Burke, Phys. Rev. Lett. **111**, 073003 (2013).
[17] L. Kronik and S. Kümmel, Phys. Chem. Chem. Phys. **22**, 16467 (2020).
[18] P. Hohenberg and W. Kohn, Phys. Rev. **136**, B864 (1964).
[19] D. Langreth and J. Perdew, Solid State Commun. **17**, 1425 (1975).
[20] J. K. Percus and G. J. Yevick, Phys. Rev. **110**, 1 (1958).
[21] L. S. Ornstein and F. Zernike, Proceedings of the Akademic Science (Amsterdam) **17**, 793 (1914).
[22] J. P. Perdew, M. Ernzerhof, and K. Burke, J. Chem. Phys. **105**, 9982 (1996).
[23] S. Van Der Walt, S. C. Colbert, and G. Varoquaux, Comput. Sci. Eng. **13**, 22 (2011).
[24] P. Virtanen, R. Gommers, T. E. Oliphant, M. Haberland, T. Reddy, D. Cournapeau, E. Burovski, P. Peterson, W. Weckesser, J. Bright, S. J. van der Walt, M. Brett, J. Wilson, K. J. Millman, N. Mayorov, A. R. J. Nelson, E. Jones, R. Kern, E. Larson, C. J. Carey *et al.*, Nat. Methods **17**, 261 (2020).
[25] S. K. Lam, A. Pitrou, and S. Seibert, in *Proceedings of the Second Workshop on the LLVM Compiler Infrastructure in HPC - LLVM '15* (Association for Computing Machinery, New York, 2015), pp. 1–6.

[26] L. H. Thomas, Math. Proc. Cambridge Philos. Soc. **23**, 542 (1927).

[27] E. Fermi, Z. Phys. **48**, 73 (1928).

[28] F. Nogueira, A. Castro, and M. A. L. Marques, A tutorial on density functional theory, in *A Primer in Density Functional Theory*, edited by C. Fiolhais, F. Nogueira, and M. A. L. Marques (Springer, Berlin, 2003), pp. 218–256.

[29] W. Pan, B. Caswell, and G. E. Karniadakis, Langmuir **26**, 133 (2010).